THE JOURNAL OF PHYSICAL CHEMISTRY A

Article

pubs.acs.org/JPCA

Raman and Infrared Spectroscopy, DFT Calculations, and Vibrational Assignment of the Anticancer Agent Picoplatin: Performance of Long-Range Corrected/Hybrid Functionals for a Platinum(II) Complex

Magdalena Malik, Rafał Wysokiński, Wiktor Zierkiewicz, Katarzyna Helios, and Danuta Michalska*

Faculty of Chemistry, Wrocław University of Technology, Smoluchowskiego 23, 50-370 Wrocław, Poland

Supporting Information

ABSTRACT: Picoplatin, *cis*-[$PtCl_2(NH_3)$(2-picoline)], is a new promising anticancer agent undergoing clinical trials, which reveals high efficacy against many tumors and greatly reduced toxicity, in comparison to cisplatin. In this work, we present for the first time the Fourier-transform Raman and infrared spectra of picoplatin, in the region of 3500−50 cm^{-1}. The comprehensive theoretical studies on the molecular structure, the nature of Pt−ligand bonding, vibrational frequencies, and intensities were performed by employing different DFT methods, including hybrid (PBE0, mPW1PW, and B3LYP) and long-range-corrected hybrid density functionals (LC-ωPBE, CAM-B3LYP). Various effective core potentials (ECP) and basis sets have been used. In the prediction of the molecular structure of picoplatin, the best results have been obtained by LC-ωPBE, followed by PBE0, mPW1PW, and CAM-B3LYP density functionals, while the least accurate is B3LYP. The use of the LanL2TZ(f) ECP/basis set for Pt, in conjunction with all tested DFT methods, improves the calculated geometry of the title complex. The PBE0, mPW1PW, and CAM-B3LYP methods have shown the best performance in the calculations of the frequencies of Pt−ligand vibrations. A clear-cut assignment of all the bands in the IR and Raman spectra have been made on the basis of the calculated potential energy distribution (PED). The nature of the "vibrational signatures" of picoplatin have been determined. These results are indispensable for further investigation on drug−target interactions using vibrational spectroscopy.

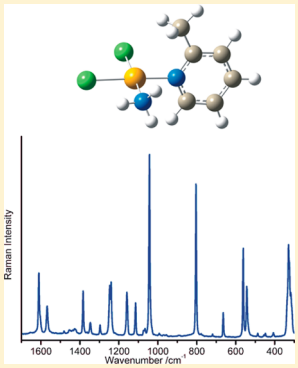

INTRODUCTION

The landmark discovery of the antitumor properties of cisplatin, *cis*-diamminedichloroplatinum(II), *cis*-[$PtCl_2(NH_3)_2$], by Barnett Rosenberg and co-workers[1] has opened the new era of platinum-based anticancer chemotherapy. Although cisplatin is one of the most successful drugs against various types of human malignancies, it shows severe dose-limiting side effects, including nephrotoxicity, neurotoxicity, and ototoxicity.[2] Moreover, many tumors display inherent resistance to cisplatin, while others develop acquired resistance after initial treatment. The second generation drugs, carboplatin, [*cis*-diammine(1,1-cyclo butanedicarboxylato)platinum(II)][3] and oxaliplatin [(1*R*,2*R*-cyclohexanediamine)oxalate platinum(II)][4] are much less nephrotoxic and neurotoxic than cisplatin, but they also have some adverse effects (myelosuppression and drug resistance). The third generation platinum-based drugs have gained regional approval in individual nations. Among them are: nedaplatin[5] in Japan; lobaplatin[6] in China; and heptaplatin[7] in South Korea. Thousands of new platinum compounds have been screened as potential antitumor agents. Unfortunately, the vast majority of these compounds have been abandoned in preclinical or clinical trials because of low efficacy or high toxicity. There are currently only a few platinum drugs in various stages of clinical trials. Among them is a very promising new agent, picoplatin.[5]

Picoplatin, *cis*-[$PtCl_2(NH_3)$(2-picoline)] (also called AMD473 or ZD0473) has demonstrated high efficacy against several tumors, including prostate and colorectal cancers. It can be applied both intravenously and orally.[8] It is remarkable that AMD473 shows anticancer activity against a wide range of cisplatin- and oxaliplatin-resistant cells.[9,10] No marked nephrotoxicity or neurotoxicity has been observed.[11] This drug seems to be close to gaining marketing approval.[5]

Picoplatin has been rationally designed to provide steric bulk around platinum. In accordance with the X-ray crystal structure of AMD473,[12] the pyridine ring is approximately perpendicular to the coordination plane ($PtCl_2N_2$) and the 2-methyl group is positioned above the platinum atom. This important structural feature introduces steric hindrance to an axial nucleophilic attack of other molecules (e.g., glutathione or water) on the Pt atom. Therefore, the rates of hydrolysis of the chloride ions in AMD473 are about 5 times slower than those of cisplatin.[12,13] The slowness of hydrolysis plays an important role in a greatly reduced toxic side effects of picoplatin, in comparison to other platinum drugs. The theoretical molecular mechanism of hydrolysis of AMD473 has been thoroughly explored by several research groups.[14−16]

It is generally accepted that platinum(II) drugs bind with DNA forming most abundantly a 1,2-intrastrand cross-link between the N7 atoms of two adjacent guanine units.[5] In the

Received: June 6, 2014
Revised: July 25, 2014
Published: July 30, 2014

dx.doi.org/10.1021/jp5056254 | *J. Phys. Chem. A* 2014, 118, 6922−6934

case of picoplatin, due to its asymmetric structure, four possible stereoisomers with DNA may exist.[17,18] Sadler and co-workers[18] performed the detailed NMR studies on the reaction of picoplatin with the 14-mer DNA duplex and demonstrated that this drug predominantly gives a single stereoisomer, where the platinum atom binds to two adjacent guanosine residues, while the 2-picoline ring fits perfectly into the major groove of the DNA duplex.

Recently, the new picoplatin-based Pt(IV) complexes with the axial ligands were obtained and revealed promising results in the treatment of malignant pleural mesothelioma (MPM).[19] A newly synthesized bromine analogue of picoplatin, *cis*-[$PtBr_2(NH_3)$(2-picoline)] has shown a similar cytotoxic activity to that of AMD473.[20]

It should be emphasized that despite the numerous studies on picoplatin, no experimental vibrational spectra of this drug have been reported hitherto. Raman spectroscopy is known to be a very sensitive tool to investigate a drug−target interaction. However, in such study, a detailed understanding of the vibrational spectra of a bare molecule is indispensable for monitoring intermolecular interactions.

The main goal of this work was to investigate the experimental Fourier transform Raman and infrared spectra of picoplatin, in the solid state. A detailed vibrational assignment has been made on the basis of the DFT calculated frequencies, infrared intensities, Raman intensities, and computed potential energy distribution (PED). The results from these calculations have enabled us to determine the nature of the characteristic "marker bands" in the spectra of picoplatin. These "vibrational signatures" can be used for further study on intermolecular interactions monitored by Raman spectroscopy. Furthermore, the spectroscopic and theoretical results obtained in this work will be helpful in the determination of the molecular structures of new derivatives of picoplatin, which are currently under investigation.

The density functional theory (DFT) has emerged as a powerful tool in computational chemistry. The DFT calculations predicting frequencies and spectral intensities are essential for interpretation of experimental spectra of molecules. In the past decade, much progress has been made in the design of new DFT methods, which have been implemented into available quantum-chemical computational programs. Zvereva et al.[21] tested the performance of three density functionals (B3LYP, M05, and M05-2X) and ab initio MP2 method for the prediction of vibrational properties of a series of small- and medium-sized organic molecules. They concluded that B3LYP is the best cost-effective choice for the prediction of harmonic frequencies and vibrational intensities of the investigated compounds. Very recently, Barone and co-workers[22] reported a thorough study on computations of fully anharmonic infrared and Raman spectra for medium-size molecular systems using the second-order vibrational perturbation theory (VPT2) and several hybrid, long-range corrected and meta-hybrid DFT functionals coupled with various basis sets. These authors demonstrated that anharmonic vibrational frequencies predicted by the B3LYP and B97-1 methods were in best agreement with the experiment. It should be noted that the tested molecules did not include the metal atoms.

In our earlier work[23] we have shown that the modified Perdew−Wang density functional model mPW1PW (mPW1PW91) introduced by Adamo and Barone[24] is remarkably superior to ab initio MP2 and other density functional protocols (including B3LYP) in a simultaneous prediction of both molecular structure and vibrational frequencies of cisplatin and carboplatin. Other studies of ours on different platinum complexes[25−27] have confirmed that the theoretical Raman and IR spectra calculated by the mPW1PW functional are in good agreement with the experimental spectra. Several research groups[28−31] investigated the use of various basis sets, effective core potentials (ECPs), and DFT methods, including mPW1PW, to determine the reliable level of calculations of molecular structures and other properties of platinum-based drugs. Recently,[32] we assessed different DFT methods, covering the range from meta-GGA to hybrid, double hybrid, and long-range corrected hybrid models (M06-L, M06, M06-2X, PBE0, mPW1PW, B3LYP, B2PLYP, CAM-B3LYP, ωB97XD, and LC-ωPBE) for their performances in the prediction of the molecular structure and vibrational spectra of cisplatin. The results have shown that LC-ωPBE is superior to other DFT methods in predicting the geometry of cisplatin.

Thus, the second purpose of this work is to compare the performance of different DFT methods, including the long-range-corrected hybrid functionals (LC-ωPBE and CAM-B3LYP) in the calculations of molecular structure and vibrational spectra of picoplatin.

METHODS

Experimental. Potassium tetrachloroplatinate(II) and potassium aminetrichloroplatinate(II) were obtained from Aldrich. 2-Methylpyridine (2-picoline) was purchased from Merck. Silver nitrate, potassium iodide, potassium chloride, concentrated hydrochloric acid, and 25% ammonia solution were supplied by POCH. All compounds were of reagent-grade purity and were used without further purification.

Two methods were employed to prepare picoplatin, *cis*-[$PtCl_2(NH_3)$(2-picoline)]. We wanted to compare which one gives a purer product (no results from elemental analysis were reported).[33] It is shown that the second method produces picoplatin of a higher purity.

Method 1. This synthesis was adapted and modified from the method described by Battle et al.[33] $K_2[PtCl_4]$ (0.50 g, 1.2 mmol) was dissolved in water (10 mL) and stirred at room temperature. Five stoichiometric equivalents of KI (1.0 g, 6 mmol) were added, and the solution was stirred until all the solid had dissolved (the flask was wrapped in aluminum foil). One stoichiometric equivalent of 2-picoline (0.12 mL, 1.2 mmol) was added slowly, and the mixture was stirred in the dark for 24 h. The obtained dark brown precipitate was separated by centrifugation and filtration. Then, 25% ammonia solution was added slowly with stirring, and the reaction was watched closely until the brown precipitate turned yellow. The obtained solid *cis*-[$PtI_2(NH_3)$(2-pic)] was collected, washed with cold water and ethyl ether, and dried in a desiccator. In the second step, *cis*-[$PtI_2(NH_3)$(2-pic)] (0.47 g, 0.83 mmol) was suspended in water (25 mL) and stirred with 2.0 stoichiometric equivalents of $AgNO_3$ (0.28 g, 1.66 mmol) for 24 h, in the dark. The silver iodide that precipitated from solution was removed by filtration. An excess of KCl (0.22 g, 2.9 mmol) was added, and the mixture was stirred for 5 h. A yellow-green precipitate of *cis*-[$PtCl_2(NH_3)$(2-pic)] was collected, washed with cold water, ethanol, ethyl ether, and placed in a desiccator. Yield 0.20 g, 0.53 mmol (44% based on $K_2[PtCl_4]$). Anal. Calc. for $C_6H_{10}N_2Cl_2Pt$: C, 19.2%; N, 7.4%; Cl, 18.9%; H, 2.7%. Found: C, 21.6%; N, 7.1%; Cl, 17.3%, H, 2.7%.

Method 2. This synthesis was adapted from the method described by Murrer.[34] KCl (0.11 g, 1.5 mmol) and

dx.doi.org/10.1021/jp5056254 | J. Phys. Chem. A 2014, 118, 6922−6934

$K[PtCl_3(NH_3)]$ (0.50 g, 1.4 mmol) were dissolved in water (10 mL) and stirred during the addition of KI (0.70 g, 4.2 mmol) in water (3 mL). Then, the stoichiometric amount of 2-picoline (0.15 mL, 1.5 mmol) was added, and the mixture was stirred in the dark for about 20 h. The yellow precipitate of *cis*-$[PtI_2(NH_3)(2\text{-pic})]$ was collected by filtration, washed with water and methanol, and dried in a desiccator. Next, *cis*-$[PtI_2(NH_3)(2\text{-pic})]$ (0.60 g, 1.1 mmol) was added to a stirred solution of $AgNO_3$ (0.37 g, 2.2 mmol) in water (10 mL) and stirring was continued for 8 h, in the dark. The silver iodide that precipitated from solution was removed by filtration. To the filtrate, the concentrated HCl (0.33 mL, 3.9 mmol) was added and stirred for 3 days. The resulting pale yellow precipitate of *cis*-$[PtCl_2(NH_3)(2\text{-pic})]$ was collected by filtration, washed with cold water and acetone, and dried in a desiccator. All steps of synthesis were conducted at room temperature. Yield 0.24 g, 0.64 mmol (43% based on $K[PtCl_3(NH_3)]$). Anal. Calc. for $C_6H_{10}N_2Cl_2Pt$: C, 19.2%; N, 7.4%; Cl, 18.9%; H, 2.7%. Found: C, 19.2%; N, 7.5%; Cl, 19.6%, H, 2.6%.

Measurements. The FT-Raman spectrum (in the range of 3500−50 cm^{-1}) was measured on a Bruker MultiRAM spectrometer equipped with a Nd:YAG laser (emitting radiation at a wavelength of 1064 nm) and a liquid nitrogen cooled germanium detector. The spectrum was recorded at a resolution of 2 cm^{-1}. The Fourier transform far-infrared (FT-FIR) and middle-infrared (FT-IR) spectra were measured on a Bruker VERTEX 70V vacuum spectrometer equipped with an air-cooled DTGS detector. The FT-IR spectrum (in the region 4000−400 cm^{-1}) was recorded in KBr pellets. For the far IR spectrum (in the range of 600−50 cm^{-1}), the diamond ATR accessory was used and the spectrum was elaborated in OPUS to convert it from reflectance into absorbance. The instrument was kept under vacuum during the measurements, and the spectra were recorded at a resolution of 2 cm^{-1}.

Theoretical. The optimized geometry, vibrational frequencies, IR intensities, and Raman scattering activities of picoplatin were calculated by five density functional methods: B3LYP, mPW1PW91, PBE0, CAM-B3LYP, and LC-ωPBE.

CAM-B3LYP[35] is a new hybrid exchange-correlation functional using the Coulomb attenuating method (this is the long-range corrected version of the B3LYP functional). LC-ωPBE[36] is a novel long-range corrected version of the hybrid ωPBE functional. Unfortunately, no Raman intensities are available for LC-ωPBE because the calculations of polarizability derivatives have not been implemented for this functional, in Gaussian 09. The mPW1PW91 protocol (hereafter abbreviated as mPW1PW)[24] is the Becke-style one-parameter hybrid model, which uses the Perdew−Wang exchange functional (modified by Adamo and Barone) and the PW91 correlation functional.[37] PBE0 (also denoted as PBE1PBE) is the one-parameter hybrid protocol, which contains the modified PBE (Perdew, Burke, Ernzerhof) exchange and correlation functionals.[38−40] B3LYP is the widely used three-parameter hybrid functional.[41,42]

In numerous papers,[23,28−31] different effective core potentials (ECPs) and basis sets were examined, in view of their prediction of molecular properties of cisplatin. In this work, we have employed two most popular ECPs, LANL2 of Hay and Wadt[43] and SDD (the Stuttgart-Dresden ECP),[44,45] which substitute the innermost core orbitals of heavy atoms and account for the relativistic effects in the core region. These potentials have been combined with the concomitant valence basis sets. In addition, we have also used the recently reported LANL2TZ(f) basis set for the Pt atom.[46] It contains the LANL2 relativistic ECP of Hay and Wadt and a flexible triple-ζ basis set augmented with (f) polarization functions in the treatment of the valence shell on the Pt atom. For the picoline and ammonia ligands, we have employed the Dunning's D95V(d,p) basis set,[47] which includes *d* polarization functions on C and N atoms and *p* polarization functions on H atoms. In our earlier studies on transition metal complexes, we have shown that the use of the D95V(d,p) basis set for atoms of the organic ligands yields very good results in the prediction of the vibrational spectra of these complexes and is the best compromise between accuracy and cost of the computations.[48−50] We also performed DFT calculations with the extended basis set for the Cl atom (using the double and triple-ζ basis set with d polarizations functions on Cl atom), but these attempts worsened the results, as the predicted Pt−Cl bond lengths were too short and the frequencies of the (Pt-Cl) stretching vibrations were too large in comparison to the experimental data. Therefore, in the present work we included only the results obtained with the LanL2DZ or SDD effective core potentials and the concomitant basis sets for the Cl atoms.

The three combinations of the basis sets are denoted as follows: I = LanL2DZ on Pt and Cl; II = SDD on Pt and Cl; III = LanL2TZ(f) on Pt and LanL2DZ on Cl. In all combinations (I, II, and III), the D95V(d,p) basis set has been used for all atoms of the ammonia and 2-picoline ligands.

The computations of the molecular structure and vibrational properties of picoplatin were performed by Gaussian 09.[51] A natural bond orbital (NBO) analysis was made using the 5.0 version of the program.[52,53]

NBO analysis provides detailed insight into the nature of electronic structure and bonding in molecules. Each natural bonding orbital, σ_{AB}, can be written in terms of two directed valence hybrids, h_A and h_B on atoms A and B, respectively, with the corresponding polarization coefficients, c_A and c_B, which vary smoothly from covalent ($c_A = c_B$) to ionic ($c_A \ll c_B$).

The interaction energy between the lone pair occupied orbital and the unoccupied σ^* orbital was estimated from the second-order perturbation theory:

$$(E^2) = -n_{\sigma LP}\frac{\langle \sigma_{LP}|F|\sigma^*\rangle^2}{\varepsilon_\sigma^* - \varepsilon_{\sigma LP}} = -n_{\sigma LP}\frac{F^2_{\sigma LP\sigma^*}}{\Delta E} \quad (1)$$

where $\langle \sigma_{LP}|F|\sigma^*\rangle$ is the Fock matrix element between the lone pair (σLP) orbital and the σ^* antibonding NBO orbital, ε_σ^* and $\varepsilon_{\sigma LP}$ are the energies of σ^* and σLP orbitals, and $n_{\sigma LP}$ is the occupancy of the donor lone pair orbital.

The calculated frequencies are usually overestimated because of the incomplete treatment of electron correlation, neglect of anharmonicity, and basis set truncation effects. To improve the agreement between calculated harmonic and observed frequencies, Schlegel and co-workers[54] introduced the "dual scaling procedure", which uses two different scale factors for the frequencies above and below 1800 cm^{-1}. The dual scaling was successfully applied by many authors in theoretical studies of the vibrational spectra.[55]

In this work, we have modified this procedure, similarly as in our earlier calculations on Pt(II) complexes.[26,27] Our approach aims at using the least possible number of scale factors, which can yield the theoretical frequencies in a good agreement with the experiment. For the PBE0 and mPW1PW methods, we have used two different scaling factors (0.942 and 0.975) for the frequencies calculated in the region above 800 cm^{-1}. Merrick et al.[56] from the IR spectra of a standard set of organic molecules

dx.doi.org/10.1021/jp5056254 | J. Phys. Chem. A 2014, 118, 6922−6934

determined similar scale factors for the theoretical frequencies calculated by the PBE0 and mPW1PW methods (0.955 and 0.953, respectively). It should be mentioned that the average of our two scaling factors (0.958) is very close to the values determined by Merrick et al. for the PBE0 functional.

Below 800 cm^{-1}, all the theoretical frequencies show quite good agreement with the experiment, therefore, we have not scaled them. Moreover, we wanted to compare the unscaled frequencies in our assessment of the performance of tested DFT methods in the predictions of the Pt−ligand vibrational modes.

To provide the detailed vibrational assignment of the experimental spectra of picoplatin, a normal coordinate analysis was carried out. The potential energy distribution (PED) was calculated at each level of theory, as described earlier.[57,58] A nonredundant set of 57 symmetrized internal coordinates has been determined, as suggested by Fogarasi et al.[59] The internal coordinates are shown in Table S1 of the Supporting Information.

The theoretical Raman intensities (I^R), which simulate the measured Raman spectrum can be calculated according to the following equations:[25,60]

$$I_i^R = C(\nu_0 - \nu_i)^4 \nu_i^{-1} B_i^{-1} S_i \quad (2)$$

where B_i is the temperature factor, which accounts for the intensity contribution of excited vibrational states, and is represented by the Boltzmann distribution:

$$B_i = 1 - \exp\left(-\frac{h\nu_i c}{kT}\right) \quad (3)$$

In equation (2), ν_0 is the wavenumber of the laser radiation (in this work, we have used ν_0 = 9398.5 cm^{-1}, which corresponds to a wavelength of the 1064 nm line of a Nd:YAG laser), ν_i is the wavenumber of the normal mode (cm^{-1}), while S_i is the computed Raman scattering activity of the normal mode Q_i. I_i^R is given in arbitrary units (C is a constant equal to 10^{-12}). As discussed earlier,[25] the factor B_i should be assumed to be 1, otherwise the calculated Raman intensities for the bands below 300 cm^{-1} are extremely overestimated, in comparison to experiment. This can be attributed to a negligible contribution of the excited vibrational states to the Raman scattering intensities of a molecule in the solid state. All the simulated spectra were plotted using a Lorentzian band shape with a half-width at half-maximum (HWHM) of 2.5 cm^{-1} (the intensities at the simulated maxima are equal to the calculated intensities).

RESULTS AND DISCUSSION

Structure. The optimized molecular geometry and the numbering of atoms of picoplatin are shown in Figure 1. The two chloride ions and two nitrogen atoms are arranged in a square-planar configuration around platinum, in agreement with the crystal structure analysis of the title complex.[12]

Table 1 lists the bond lengths and bond angles of the Pt coordination sphere calculated by the B3LYP, CAM-B3LYP, LC-ωPBE, PBE0, and mPW1PW density functional methods using the I, II, and III basis sets (the notations for the combined basis sets are described in the footnotes of Table 1). In accordance with the results obtained by all DFT methods, the Pt−Cl5 bond (in the *cis* position to the coordinated pyridine ring) is longer by about 0.01 Å than the *trans* Pt−Cl4 bond. Thus, in a bare picoplatin in the gas phase, the presence of the methyl group in axial position causes an elongation of the Pt−Cl5 bond. In crystal, however, the difference between the two Pt−Cl bonds is about 0.02 Å (with Pt−Cl5 being shorter than the Pt−Cl4 bond). This is caused by the strong intermolecular N−H···Cl hydrogen bonds between the three H atoms of the NH_3 ligand and four Cl ligands from two neighboring molecules.[12] Therefore, the average experimental and the average theoretical Pt−Cl bond lengths (calculated at each level of theory) are compared in Table 1.

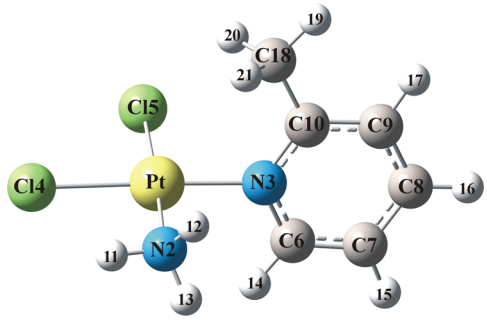

Figure 1. Optimized molecular geometry and the numbering of atoms of picoplatin.

To assess the performance of the theoretical methods in the prediction of the molecular structure of picoplatin, we have investigated the following criteria: individual differences (d) between the calculated and experimental values of a geometrical parameter; and mean percent deviations (Δ), as suggested by Amado et al.[28] The (d) and (Δ) values are provided in Table 1.

As is seen in Table 1 (and in Figure S1 of the Supporting Information), for all the investigated DFT methods, the use of the I basis set yields the largest deviations between the calculated and experimental Pt−ligand atom distances, Δr_{Pt-L}. The II basis set gives a better agreement with the experiment. However, the most accurate results are obtained with the III basis sets, regardless of the DFT method used (the III basis set includes the LanL2TZ(f) basis set for Pt).

Of all the levels of theory, the popular B3LYP method with I basis set gives the biggest differences with respect to the experiment, the overall mean percent deviation for bond lengths, Δr_{Pt-L} is 3.6%, while Δ_A for bond angles is 3.9%. As follows from the examination of the individual differences (d) in Table 1, the B3LYP/I level significantly overestimates the Pt−Cl atom distances (by about 0.10 Å). Also, the calculated Pt−N2 and Pt−N3 atom distances are too long, by about 0.08 and 0.05 Å, respectively. The CAM-B3LYP method gives a better agreement with the experiment than B3LYP, the values of Δr_{Pt-L} are between 2.7% and 1.9% for the I and III basis sets, respectively. Very good results have been obtained at the PBE0/III and mPW1PW/III levels of theory, and the Δr_{Pt-L} values are 1.2% and 1.4%, respectively. As is evident from Table 1, the LC-ωPBE/III level of theory performs the best in the prediction of the platinum−ligand bond lengths, the mean percent deviation Δr_{Pt-L} is only about 1.0%.

Thus, from the comparison of the results obtained by the III basis set, we find that ranking of the tested functionals ordered according to decreasing values of Δr_{Pt-L} is B3LYP > CAM-B3LYP > mPW1PW ~ PBE0 ~ LC-ωPBE.

Certainly, one should be aware of the fact that we cannot expect a perfect agreement between the corresponding theoretical and experimental bond lengths and bond angles because the calculated results refer to the molecule in the gas phase at 0 K, whereas the experimental data have been obtained

dx.doi.org/10.1021/jp5056254 | J. Phys. Chem. A 2014, 118, 6922−6934

Table 1. Comparison of the Structural Parameters (Distances in Å, Angles in Degrees) of Picoplatin Calculated with Different DFT Methods Using Various Basis Sets (I, II, and III).

method[a]	r(Pt−Cl)[b]	$d_{Pt\text{-}Cl}$[c]	r(Pt−N2)	$d_{Pt\text{-}N2}$[c]	r(Pt−N3)	$d_{Pt\text{-}N3}$[c]	Δr[d]	∠ClPtCl	d_{ClPtCl}[c]	∠NPtN	d_{NPtN}[c]	∠N3PtCl5	$d_{N3PtCl5}$[c]	Δ_A[d]	Δ_{all}[e]
B3LYP/I	2.410	0.100	2.110	0.080	2.067	0.050	3.6	95.0	2.4	95.8	5.3	86.6	−2.9	3.9	3.7
B3LYP/II	2.395	0.085	2.106	0.076	2.064	0.047	3.2	94.5	1.9	95.4	4.9	87.0	−2.5	3.4	3.3
B3LYP/III	2.385	0.075	2.095	0.065	2.047	0.030	2.6	94.5	1.9	95.3	4.8	87.2	−2.3	3.3	3.0
CAM-B3LYP/I	2.391	0.081	2.090	0.060	2.053	0.036	2.7	95.1	2.5	95.5	5.0	86.5	−3.0	3.9	3.3
CAM-B3LYP/II	2.374	0.064	2.086	0.056	2.051	0.034	2.4	94.7	2.1	95.1	4.6	86.8	−2.7	3.5	3.0
CAM-B3LYP/III	2.365	0.055	2.076	0.046	2.036	0.019	1.9	94.7	2.1	95.0	4.5	86.9	−2.6	3.4	2.6
LC-ωPBE/I	2.370	0.060	2.073	0.042	2.036	0.019	1.9	94.8	2.2	95.4	4.9	86.4	−3.1	3.8	2.8
LC-ωPBE/II	2.352	0.042	2.068	0.038	2.034	0.017	1.5	94.4	1.8	95.0	4.5	86.7	−2.8	3.3	2.4
LC-ωPBE/III	2.344	0.033	2.059	0.029	2.020	0.003	1.0	94.4	1.8	94.9	4.4	86.8	−2.7	3.3	2.2
PBE0/I	2.384	0.074	2.080	0.050	2.036	0.019	2.2	94.7	2.1	95.8	5.3	86.6	−2.9	3.8	3.0
PBE0/II	2.367	0.057	2.076	0.046	2.034	0.017	1.9	94.3	1.7	95.4	4.9	87.0	−2.5	3.3	2.6
PBE0/III	2.357	0.047	2.065	0.035	2.016	−0.001	1.2	94.2	1.6	95.2	4.7	87.2	−2.3	3.2	2.2
mPW1PW/I	2.389	0.079	2.083	0.053	2.039	0.022	2.4	94.6	2.0	95.8	5.3	86.7	−2.8	3.7	3.0
mPW1PW/II	2.368	0.058	2.079	0.049	2.037	0.020	2.0	94.3	1.7	95.4	4.9	87.0	−2.5	3.3	2.6
mPW1PW/III	2.359	0.049	2.068	0.038	2.020	0.003	1.4	94.2	1.6	95.2	4.7	87.2	−2.3	3.2	2.3

[a]Notations for basis sets: I = LanL2DZ on Pt and Cl; II = SDD on Pt and Cl; III = LanL2TZ(f) on Pt, LanL2DZ on Cl. In all cases, the D95V(d,p) basis set was used for N, C, and H atoms. [b]The average of two calculated Pt−Cl bond lengths. The two theoretical values differ by less than 0.010 Å. [c]Difference between the calculated and the corresponding experimental values. For the Pt−Cl bond lengths, the average of experimental X-ray crystal data were used: r(Pt−Cl) = 2.310 Å [2.299(2) and 2.322(2) Å]; r(Pt−NH_3) = 2.030(8) Å; r(Pt−N_{py}) = 2.017(8) Å; bond angles: Cl−Pt−Cl = 92.70(8)°, N−Pt−N = 90.5(3)° and N_{py}−Pt−Cl5 = 89.5(2)°.[12] [d]Mean percent deviations for bond lengths (Δr) or bond angles (Δ_A) are obtained by the following equation:

$$\Delta = \frac{\sum_{i=1}^{n} (|y_i - x_i|/x_i)}{n} \times 100$$

where y_i and x_i are the theoretical and experimental structural parameters, respectively, and n = total number of structural parameters considered. [e]Overall mean percent deviations for all structural parameters considered.

Table 2. Comparison of Experimental and Theoretical Bond Lengths (Å) and Angles (°) of Picoplatin Calculated by Different DFT Methods with III Basis Set.

	exptl[a]	B3LYP	CAM- B3LYP	LC-ωPBE	PBE0	mPW1PW
R(N3−C10)	1.344(5)	1.361	1.353	1.348	1.355	1.355
R(C6−C7)	1.381(6)	1.391	1.385	1.381	1.387	1.386
R(C7−C8)	1.376(8)	1.400	1.395	1.392	1.395	1.395
R(C8−C9)	1.369(7)	1.396	1.390	1.386	1.391	1.391
R(C9−C10)	1.391(5)	1.404	1.398	1.395	1.399	1.399
R(C10−C18)	1.495(7)	1.503	1.499	1.496	1.494	1.495
Δr[b]		1.12	0.70	0.46	0.76	0.74
∠PtN3C6	117.6(3)	117.6	117.7	117.9	117.9	117.9
∠PtN3C10	123.3(2)	122.7	122.5	122.2	122.3	122.3
∠N3C6C7	122.4(5)	122.9	122.9	122.9	122.9	122.9
∠N3C10C9	120.1(3)	119.9	120.0	120.0	119.9	119.9
∠N3C10C18	118.5(3)	118.9	118.9	118.5	118.6	118.7
∠C6C7C8	118.4(5)	118.4	118.3	118.2	118.4	118.4
∠C7C8C9	119.3(5)	118.6	118.7	118.8	118.6	118.6
∠C8C9C10	120.6(4)	120.7	120.5	120.4	120.6	120.6
∠C6N3C10	119.2(4)	119.5	119.6	119.7	119.7	119.7
∠C10N3PtN2	102.7	103.4	103.3	103.3	103.6	103.2
Δ_{all}[c]		0.72	0.51	0.41	0.57	0.54

[a]X-ray crystal data[12] (collected from CCDC-100573) [b]Mean percent deviations for bond lengths (equation indicated below Table 1). [c]Overall mean percent deviations for all structural parameters.

for the crystal structure of picoplatin, where intermolecular interactions (hydrogen bonds and packing forces) can affect the geometrical parameters. The theoretical results indicate that in a bare picoplatin there is a weak intramolecular C18−H20···Cl5 hydrogen bonding (the distance between H20 and Cl5 is equal 2.77 Å, which is smaller than the sum of the corresponding van der Waals radii, by 0.18 Å). This electrostatic interaction leads to a decrease of the N3−Pt−Cl5 angle with a simultaneous

dx.doi.org/10.1021/jp5056254 | J. Phys. Chem. A 2014, 118, 6922−6934

increase of both the N−Pt−N and Cl−Pt−Cl angles, relative to the corresponding experimental data. In the crystal of picoplatin, the intermolecular N−H···Cl hydrogen bonds become more important, therefore, the experimental values of both the N−Pt−N and Cl−Pt−Cl bond angles are smaller (and consequently, the N−Pt−Cl angles are bigger) than the corresponding bond angles calculated for the gas phase, at all levels of theory. The theoretical Cl−Pt−Cl angle varies in the range from 94.2° (mPW1PW/III and PBE0/III) to 95.1° (CAM-B3LYP/I), whereas the experimental value is equal to 92.70(8)°.[12] The calculated N3−Pt−Cl5 angle is smaller than the experimental, and the differences (d_{NPtCl}) are in the narrow range between −3.1° and −2.3°. As is seen in Table 1, the calculated mean percent deviations for bond angles, Δ_A, are very similar for all the examined methods (between 3.2 and 3.9%).

Table 2 collects the experimental and calculated atom distances and bond angles of the 2-methylpyridine (2-picoline) ligand in the complex. The comparison is made for all investigated DFT methods using only the III basis set. The most notable structural feature of picoplatin is the nearly perpendicular orientation of the pyridine ring with respect to the coordination plane. The experimental dihedral angle (102.7°)[12] is very well-reproduced by all theoretical methods, and the calculated C10N3PtN2 torsional angle varies between 103.2 and 103.6° (Table 2).

As follows from Table 2, of all the DFT methods assessed in this study, the LC-ωPBE functional performs the best for the prediction of bond lengths in the picoline ligand. For example, the calculated N3-C10 (1.348 Å) and C10-C18 (1.496 Å) atom distances are in excellent agreement with the experimental values [1.344(5) and 1.495(7) Å, respectively]. The mean percent deviation for bond lengths (Δ_r) is less than 0.5% at this level of theory.

Thus, it can be concluded that the long-range corrected functional, LC-ωPBE (combined with the III basis set), is superior to other DFT methods for the prediction of bond lengths in picoplatin. However, very good results are also obtained with the PBE0, mPW1PW, and CAM-B3LYP methods. It should be emphasized that very similar results have been obtained in our recent studies on cisplatin.[32]

NBO Analysis. The natural bond orbital analysis (NBO) of *cis*-[$PtCl_2(NH_3)$(2-picoline)] was performed using the PBE0 exchange-correlation functional with the III basis set. Additional NBO analysis of cisplatin has been done at the same level of theory, for comparison with picoplatin. The calculated natural charges on the corresponding atoms of the two platinum complexes are listed in Table S2 of the Supporting Information.

The charges located on the platinum atom, two chloride ligands (Cl4 and Cl5), and the nitrogen atom of the ammonia ligand (N2) in picoplatin are very similar to those on the corresponding atoms of cisplatin. However, the charge on the N3 atom of the picoline ligand is more positive, by +0.53 e, than that on the ammonia nitrogen atom. This effect is caused by a strong electron delocalization within the pyridine ring.

The selected NBO orbitals, its description, and occupancy are presented in Table 3. According to these results, the σ(Pt-Cl) natural bonding orbital can be written in terms of two directed valence hybrids. In cisplatin, the σ(Pt−Cl) bond is formed from an overlap of the $sd^{1.2}$ hybrid on the platinum atom (which is the mixture of 45.8% s, 0.5% p, and 53.7% d atomic orbitals) and the $sp^{8.1}$ hybrid on the Cl atom (11.0% s and 89.0% p). In the case of picoplatin, the σ(Pt-Cl4) and σ(Pt-Cl5) bonding orbitals are formed by an overlap of the $sd^{1.2}$ hybrid on platinum (very similar to that in cisplatin) with the $sp^{7.1}$ (87.7% p) and $sp^{7.8}$ (88.7% p) hybrids on the Cl4 and Cl5 atoms, respectively. As follows from the NBO analysis, in both the complexes, the σ(Pt−Cl) bonds are strongly polarized toward the Cl atoms, with about 76% of electron density concentrated on the chlorine atom. The calculated total electron population (occupancy) on σ(Pt−Cl) orbitals is about 1.97 e.

Table 3. Selected NBO Orbitals of *cis*-[$PtCl_2(NH_3)$(2-picoline)] and *cis*-[$PtCl_2(NH_3)_2$], Their Description and Occupancy (e), Second-Order Interaction Energies (E^2, kcal mol^{-1}) between Donor and Acceptor Orbitals[a]

molecule	NBO orbital[b]	description of the orbital	occupancy	E^2
picoplatin	σ(Pt-Cl4)	$0.488(sd^{1.2})_{Pt} + 0.873(sp^{7.1})_{Cl4}$	1.972	
	σ(Pt-Cl5)	$0.503(sd^{1.2})_{Pt} + 0.864(sp^{7.8})_{Cl5}$	1.968	
	LP(N2)	$sp^{4.6}$	1.713	
	LP(N3)	$sp^{3.3}$	1.660	
		LP(N2) →σ*(Pt-Cl5)[c]		116
		LP(N3) →σ*(Pt-Cl4)[c]		124
cisplatin	σ(Pt-Cl)	$0.494(sd^{1.2})_{Pt} + 0.869(sp^{8.1})_{Cl}$	1.971	
	LP(N)	$sp^{4.5}$	1.709	
		LP(N) →σ*(Pt-Cl)[c]		118

[a]Calculations performed at the PBE0/III level. [b]σ_{AB} is a natural sigma bonding orbital, LP(N) is a lone pair orbital of nitrogen atom. [c]Donor and acceptor orbitals.

As is seen in Table 3 for picoplatin, the lone pair orbital, LP(N2), on the ammonia nitrogen atom is an $sp^{4.6}$ hybrid. It has 82.1% p character and is occupied by 1.713 electrons. Similarly, in cisplatin, the corresponding LP(N) orbital on the nitrogen atom is the $sp^{4.5}$ hybrid (81.9% p character) and is occupied by 1.709 e.

In picoplatin, the lone pair orbital on the N3 nitrogen atom of the pyridine ring, LP(N3), has 76.7% p character and is occupied by 1.660 e. A decrease in occupancy of the LP(N3) orbital (from the idealized occupancy of 2.0 e) is due to a delocalization of electron density from LP(N3) to the aromatic pyridine ring.

As revealed by NBO, in both the platinum complexes, the interaction between platinum and the nitrogen atoms (in the NH_3 group or in the pyridine ring) can be described as the (N→Pt) coordination bond. This interaction corresponds to a donation of electron density from the lone pair orbital on the nitrogen atom, LP(N), to the antibonding σ*(Pt−Cl) orbital, in the trans position. The strength of this donor−acceptor interaction is estimated by the second-order interaction energy (E^2), as defined by eq (1). For cisplatin, the value of E^2 for the LP(N)→σ*(Pt−Cl) is 118 kcal mol^{-1} (for each bond), while for picoplatin, E^2 values of the LP(N2)→σ*(Pt−Cl5) and LP(N3)→σ*(Pt−Cl4) interactions are 116 and 124 kcal mol^{-1}, respectively.

Thus, the strength of the N(donor)→Pt(acceptor) interactions seems to be the largest for the LP(N3)→σ*(Pt−Cl4) donation. Moreover, additional stabilizing effects arise from the interactions between the lone pair orbital of each of the N atoms and antibonding Rydberg orbitals of Pt. In cisplatin, the sum of the E^2 energies of the LP(N)→Σ RY*Pt interactions is 35 kcal mol^{-1} (for each Pt−N bond). In the case of picoplatin,

dx.doi.org/10.1021/jp5056254 | J. Phys. Chem. A 2014, 118, 6922−6934

Table 4. Experimental Bands in the IR and Raman Spectra and the Theoretical Frequencies, ν (cm^{-1}), IR intensities, I_{IR} (km mol^{-1}), Raman Scattering Activities, S_R ($Å^4$ amu^{-1}), Raman Intensities (Arbitrary Units) and Vibrational Assignments of Picoplatin

	exptl[a]		mPW1PW	PBE0				
no.	IR	Raman	ν^b	ν^b	I_{IR}	S_R	I_R^c	PED[a,d]
1	3260 m		3429	3422	35.8	35.0	4.6	ν_a^I (NH_3)(78), ν_a^{II} (NH_3)(22)
2	3190 m	3198 w	3378	3370	41.0	45.1	6.1	ν_a^{II} (NH_3)(62), ν_a^I (NH_3)(17)
3	ov	3135 w	3238	3231	38.3	97.3	15.4	ν_s (NH_3)(79), ν_a^{II} (NH_3)(16)
4	3080 vw	3079 m	3082	3077	1.5	186.8	34.5	ν (C7−H15)(+62), ν (C6−H14)(+29)
5	3066 w	3067 m	3071	3065	1.8	96.6	17.5	ν (C9−H17)(+61), ν (C8−H16)(+22), ν (C6−H14)(−16)
6		3060 sh	3067	3062	0.9	58.1	10.9	ν (C6−H14)(+52), ν (C7−H15)(−28), ν (C9−H17)(+19)
7	3045 sh	3047 w	3053	3047	1.4	47.4	9.0	ν (C8−H16)(−70), ν (C9−H17)(+18), ν (C7−H15)(+10)
8	2973 w	2975 w	3007	3003	15.5	50.2	10.0	ν_a^I (CH_3)(99)
9	2945 w	2947 w	2977	2971	3.8	31.7	6.5	ν_a^{II} (CH_3)(99)
10		2905 m	2901	2895	10.8	152.6	33.9	ν_s (CH_3)(98)
11	1653 w		1670[e]	1664[e]	29.8	5.6	5.1	δ_a^I (NH_3) (71), δ_a^{II} (NH_3)(28)
12	ov		1645[e]	1638[e]	31.0	7.8	7.4	δ_a^{II} (NH_3)(70), δ_a^I (NH_3)(28)
13	1611 s	1611 s	1591	1591	19.4	58.3	52.0	ν (C6−C7)(−22), ν (C9−C10)(−21),ν (C8−C9)(+17)
14	1566 m	1568 m	1550	1550	10.6	15.3	14.4	ν (C7−C8)(−34), ν (N3−C10)(−16), ν (C8−C9)(+14)
15	1479 vs	1480 vw	1493	1491	46.6	4.2	4.5	δ (C6−H14)(−21), δ (C9−H17)(+17), ν ring (35)
16	1452 s	1455 vw	1463	1459	34.6	3.5	3.8	δ_a^I (CH_3)(35), δ (C7−H15)(+14)
17	1425 w	1427 w	1432	1425	13.6	7.7	8.9	δ_a^{II} (CH_3)(83)
18	1417 w	ov	1420	1414	7.9	1.0	1.2	δ_a^I (CH_3)(40), δ (C7−H15)(+13), δ (C8−H16)(+10)
19	1382 m	1383 m	1382	1376	9.6	12.9	15.9	δ_s (CH_3)(84)
20	1324 vs		1289[e]	1285[e]	158.8	2.2	3.2	δ_s (NH_3)(100)
21	ov	ov	1302	1306	2.7	8.2	11.0	ν (N3−C10)(+31), ν (N3−C6)(−17), ν (C9−C10)(−13)
22	1294 w	1296 w	1289	1285	7.2	1.3	1.8	δ (C6−H14)(+41), δ (C9−H17)(+26), ν (N3−C6)(+15)
23	1240 w	1243 m	1245	1244	1.6	26.0	37.7	ν (C10−C18)(+31), δ ring (23), δ_s (CH_3)(11)
24	1156 m	1159 m	1152	1149	3.8	5.2	8.6	δ (C8−H16)(−38), δ (C7−H15)(+24), δ (C9−H17)(+19)
25	1113 m	1114 m	1116	1113	5.2	7.6	13.3	δ (C7−H15)(+32), ν (C6−C7)(+15), δ (C9−H17)(−13)
26	1064 w	1066 vw	1066	1065	3.5	11.0	20.5	ν (C7−C8)(+34), ν (C6−C7)(+15), δ ring (10)
27	ov	1043 vs	1035	1035	0.1	51.6	100.0	δ R1 (47) ('star of David'), ν ring (40)
28	1036 m	ov	1033	1030	8.9	3.4	6.7	rock^{II} (CH_3)(70), γ (C10−C18)(−15)
29	ov	ov	991	988	0.6	0.4	0.9	γ (C8−H16)(−53), γ (C7−H15)(+24), γ (C9−H17)(+17)
30	991 vw	993 vw	989	988	0.7	1.6	3.4	rock^I (CH_3)(67), γ (C8−H16)(−11)
31	957 vw	956 vw	960	956	0.3	0.4	0.9	γ (C6−H14)(+72), γ (C7−H15)(−19), γ (C8−H16)(−11)
32	881 vw	892 vw	875	872	0.3	0.1	0.3	γ (C9−H17)(−53), γ (C7−H15)(+26), γ (C6−H14)(+19)
33	840 br		801[e]	801[e]	23.8	14.4	41.7	rock^{II} (NH_3)(68), rock^I (NH_3)(24)
34	803 m	804 vs	801	802	0.7	27.6	77.4	δ ring (53), ν(C10−C18)(30)
35	778 vs	778 vw	782	779	55.2	0.4	1.2	τ R1(24), γ(C7−H15)(−24), γ(C8−H16)(−24), γ(C9−H17)(−16)
36	ov		762	762	5.5	0.2	0.7	rock^I (NH_3)(71), rock^{II} (NH_3)(24)
37	717 s	719 vw	738	737	14.0	1.3	4.3	τ R1(61), γ (C10−C18)(11)
38	664 w	665 m	670	668	0.4	9.6	35.7	δ R2(62), δ R3(13)
39	560 w	562 s	565	565	0.3	8.7	40.0	δ R3(59), ν(C10−C18)(+17)
40	541 w	544 m	501	501	0.9	1.5	7.8	τ R3(40), τ R1(20), γ (C10−C18)(20)
41	484 m	487 w	484	487	8.4	5.8	32.0	ν (Pt−N2)(86)
42	454 m	455 vw	457		2.8	0.5	3.1	τ R2(63), γ (C10−C18)(15), γ (N3-Pt)(14)
	447 m	448 w		457				
43	406 vw	407 w	406	407	1.7	0.2	1.2	δ (C10−C18)(75)
44	330 vs (324 m)[f]	329 s (325sh)[f]	341	342	24.9	9.9	83.0	ν (Pt−Cl5)(+73), ν (Pt−Cl4)(+23); ν_s (Pt-Cl)
45	317 vs (311 s)[f]	318 m (311sh)[f]	329	330	35.7	8.9	77.9	ν (Pt−Cl4)(+73), ν (Pt−Cl5)(−25); ν_a (Pt-Cl)
46	258 m	264 m	255	255	1.2	1.9	22.0	τ R2(41), γ (C10−C18)(23), δ (Pt−N2)(−14)
47	242 m	244 w	238	239	6.0	0.6	7.3	δ (Cl5−Pt−N3)(+38), ν (Pt−N3)(−30), δ (Pt−N2)(+10)
48	228 m	228 m	218	219	4.8	0.6	7.9	π_s Pt(45), δ (N3−Pt)(+31), δ (Cl5−Pt−N3)(+21)
49	202 sh	207 m	201	202	1.1	1.0	15.8	ν (Pt−N3)(−30), δ (Cl5−Pt−N3)(−22), δ (N3−Pt)(+17)
50	193 m	ov	173	176	1.3	0.5	9.6	τ (CH_3)(70), τ R3(13), δ (Pt−N2)(13)
51	178 w	184 s	153	154	1.8	1.4	28.7	τ R3(39), π_b Pt (16), δ (Cl−Pt−Cl)(11)
52	169 w	ov	145	146	4.0	0.2	4.3	π_b Pt (85)
53	164 sh	164 m	141	141	1.3	2.2	49.8	δ (Cl−Pt−Cl)(−80), δ (Pt−N2)(+14)
54	ov	ov	98	99	0.3	0.8	27.1	τ (NH_3)(57), π_s Pt (40)
55	120 m	126 vs	65	66	5.3	2.3	114.5	π_s Pt (72), τ (NH_3)(24)
56	105 m	100 sh	59	58	1.6	2.7	151.7	γ (N3−Pt)(30), π_s Pt (30), τ ring (18)

dx.doi.org/10.1021/jp5056254 | J. Phys. Chem. A 2014, 118, 6922−6934

Table 4. continued

	exptl[a]		mPW1PW	PBE0				
no.	IR	Raman	ν^b	ν^b	I_{IR}	S_R	I_R^c	PED[a,d]
57	94/80 s	84 vs	50	51	3.3	6.2	395.9	τ (ring/coor.)(77), γ (N3−Pt)(16)
	65 vs							lattice
	57 s							lattice

[a]Abbreviations: br, broad; m, medium; ov, overlapped bands; s, strong; sh, shoulder; w, weak; v, very; ν, stretching; δ, in-plane bending or NH_3 deformation; γ, out-of-plane bending; ρ_r, rocking; τ, torsion; π_b and π_s are boat-type and saddle-type (PtN_2Cl_2) deformations, respectively (see Table S1 of the Supporting Information). Subscripts: *a*, antisymmetric; *s*, symmetric. [b]Two scaling factors for the calculated harmonic frequencies have been used: 0.942 for modes 1−10, 13, 14; 0.975 for modes 15−34. Other calculated frequencies are left unscaled (see text). [c]A scaling factor of 0.426 was used to normalize the calculated Raman intensities. The Raman intensity of mode 27 calculated by eq (2) was assumed to be 100%. [d]The predominant components of the PED matrix or their linear combinations (e.g., stretching or bending of the ring). The (+) sign corresponds to a simultaneous elongation (or a simultaneous contraction) or the clockwise in-plane bending or the in-phase out-of-plane bending of the A−B bonds. The (−) sign has the opposite meaning. The PED elements calculated by the mPW1PW method are almost identical to those from PBE0 calculations. [e]The theoretical frequencies of ammonia bending and rocking vibrations are unscaled. [f]Possible Davydov effect (see text).

the corresponding sums of the E^2 energies of the LP(N2)→Σ RY*Pt and LP(N3)→Σ RY*Pt interactions are 55 and 49 kcal mol^{-1}, respectively. As follows from these results, the N→Pt coordination bonds are slightly stronger in picoplatin, in comparison to cisplatin.

Vibrational Spectra. Theoretical vibrational spectra of picoplatin have been computed by the mPW1PW, PBE0, B3LYP, CAM-B3LYP, and LC-ωPBE density functional methods using the III basis set (however, no Raman intensities could be calculated by the LC-ωPBE method, as mentioned in Theoretical). All the theoretical results obtained with the five DFT methods are gathered in Table S3 of the Supporting Information.

Table 4 lists the experimental and theoretical frequencies, IR intensities, Raman scattering activities, and Raman intensities calculated at the PBE0/III level. In addition, the mPW1PW/III calculated frequencies are also included, for comparison.

The last column of Table 4 summarizes the predominant elements of the calculated potential energy distribution (PED). These results are indispensable for making the unequivocal assignments of all the bands in the experimental spectra of picoplatin.

2-Picoline (2-Methylpyridine) Ligand Vibrations. Figure 2 shows the experimental Raman and infrared absorption spectra of picoplatin, in the range from 3500 to 500 cm^{-1}. Figure 3 compares the experimental Raman spectra, in the region 1800−900 cm^{-1}, with the corresponding theoretical Raman spectra calculated by the B3LYP, CAM-B3LYP, mPW1PW, and PBE0 density functional methods using the III basis set. As is seen from this comparison, the relative Raman intensities of the bands in this range are fairly well-predicted by all the theoretical methods.

In the experimental Raman spectrum (Figure 2), the strongest band is observed at 1043 cm^{-1}. In accordance with the calculated PED, this band corresponds to the mode 27, which can be described as the trigonal ring breathing or the "Star of David" vibration of the 2-picoline ring. The calculations predict very large Raman intensity and very small IR intensity of this mode, in conformity with the experimental data.

The next very strong Raman band at 804 cm^{-1} (Figure 2) is assigned to the mode 34. It has the predominant contribution (53%) from the in-plane ring bending vibration mixed with the ν(C−CH_3) stretching vibration (30%), as shown in Table 4. This assignment is supported by the calculated large Raman intensity of mode 34. The theoretical frequencies, 801 cm^{-1} (mPW1PW) and 802 cm^{-1} (PBE0), are very similar to each other and both these values are very close to the experiment.

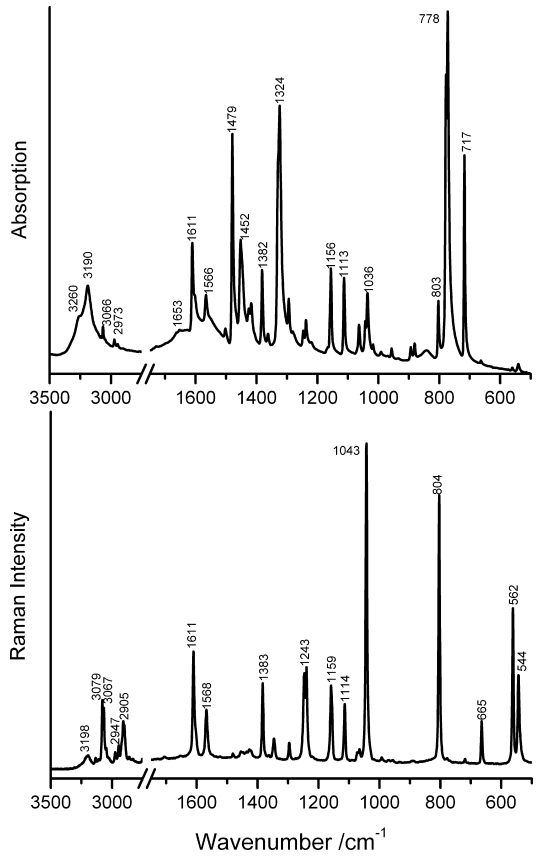

Figure 2. Experimental FT-IR spectrum (upper part) and FT-Raman spectrum (lower part) of picoplatin (range 3500−500 cm^{-1}).

In the infrared spectrum (Figure 2), the strongest band appears at 778 cm^{-1}. In accordance with the calculations, this band is due to the picoline ring torsion coupled with the γ(C−H) out-of-plane bending vibrations (mode 35). This assignment is based on the predicted large infrared intensity of mode 35 and is also supported by the excellent agreement between the experimental (778 cm^{-1}) and the theoretical unscaled frequencies, 782 and 779 cm^{-1} (from the mPW1PW and PBE0 calculations, respectively). The neighboring strong IR band at 717 cm^{-1} arises from the mode 37 (ring torsion vibration). It is worth mentioning that the calculations predict very small Raman intensities for both the modes 35 and 37. Indeed, in the experimental Raman spectrum, the corresponding bands at 778 and 719 cm^{-1} are very weak.

dx.doi.org/10.1021/jp5056254 | J. Phys. Chem. A 2014, 118, 6922−6934

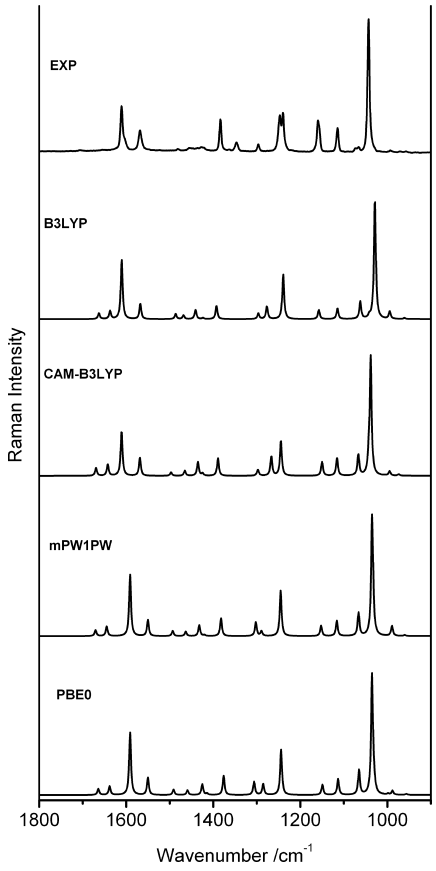

Figure 3. Comparison between the experimental Raman spectrum of picoplatin (range 1800−900 cm^{-1}) and the corresponding theoretical Raman spectra calculated by the B3LYP, CAM-B3LYP, mPW1PW, and PBE0 methods using the III basis set.

In accordance with PED, the very strong band at 1479 cm^{-1} in the IR spectrum should be assigned to the δ(C−H) in-plane bending vibrations coupled with the stretching vibration of the picoline ring (mode 15).

To assign the ν(C−H) stretching vibrations, we have compared the calculated and experimental frequencies and the relative Raman intensities of the bands. The bands in the range of 3080−3040 cm^{-1} are assigned to the ν(C−H) stretching vibrations of the picoline ring, whereas the bands in the range of 2975−2900 cm^{-1} arise from the $\nu(CH_3)$ stretching vibrations of the methyl group.

The distinct Raman band at 2905 cm^{-1} (Figure 3) is undoubtedly associated with the $\nu_s(CH_3)$ symmetric stretching vibration. It should be mentioned that in the Raman spectrum of solid 1-methylthymine, the corresponding $\nu_s(CH_3)$ band was assigned at a very similar wavenumber, 2901 cm^{-1}.[61]

Ammonia Ligand Vibrations. In the IR spectrum (Figure 2), the two broad bands at 3260 and 3190 cm^{-1} are due to the $\nu(NH_3)$ stretching vibrations of the ammonia ligand in picoplatin (modes 1 and 2, respectively). These bands occur at lower wavenumbers, in comparison to the corresponding bands at 3285 and 3206 cm^{-1} reported for cisplatin.[32] Such a red shift of the N−H stretching frequencies in picoplatin indicates that the intermolecular N−H···Cl hydrogen bonds in the crystal of picoplatin are slightly stronger than those in the solid cisplatin.

The very strong band at 1324 cm^{-1} in the IR spectrum is undoubtedly associated with the $\delta_s(NH_3)$ symmetric bending vibration, also called umbrella vibration (mode 20). It should be emphasized that this band is the characteristic "spectral signature" of the ammonia ligand in picoplatin. The predicted harmonic frequencies of $\delta_s(NH_3)$ are lower than the experimental by 35 and 39 cm^{-1}, in the mPW1PW and PBE0 calculations, respectively (Table 4). However, the calculated infrared intensity of this mode is extremely overestimated, in the harmonic approximation. All the DFT methods consistently yielded for mode 20 the largest IR intensity of all the normal modes of picoplatin (see Table S3 of the Supporting Information). On the other hand, the calculated Raman intensity of mode 20 is very small.

In our study on cisplatin,[32] we have obtained similar results. In the IR spectrum of cisplatin, the strong bands at 1314 and 1299 cm^{-1} were assigned to two NH_3 umbrella vibrations. In the harmonic approximation, the calculations at the PBE0/III level predicted the corresponding frequencies at 1298 and 1292 cm^{-1}, respectively (the accidentally good agreement of these values with experiment was due to some error cancellation). However, the theoretical infrared intensities were much too large, in comparison to the experiment. On the other hand, in the anharmonic approximation, the PBE0/III method yielded these frequencies at 1248 and 1242 cm^{-1}, respectively (they were too low by about 60 cm^{-1}, in comparison with the experiment).

On the basis of the results obtained in this work and those reported earlier for cisplatin,[32] we can conclude that the symmetric bending (umbrella) mode of the ammonia group in platinum(II) complexes is probably a large-amplitude vibration (LAV), therefore, neither the harmonic nor the anharmonic approximation can reliably predict the wavenumber of this mode.

Platinum-Ligand Vibrations. Figure 4 illustrates the experimental FT-Raman and FT-IR spectra of picoplatin in the 500−100 cm^{-1} region.

In the IR spectrum, the strongest bands occur at 317 and 330 cm^{-1}. Each of the two bands shows a splitting into two peaks of different intensities. A similar effect is observed in the Raman spectrum, each of the two bands at 318 and 329 cm^{-1} has a shoulder (at 311 and 325 cm^{-1}, respectively). According to the calculated PED, the higher wavenumber band, 330/329 cm^{-1} (IR/Raman), is assigned to the ν_s(Pt−Cl) symmetric (or the in-phase) stretching vibration (mode 44), while the other one, 317/318 cm^{-1} (IR/Raman) arises from the ν_a(Pt−Cl) antisymmetric (or the out-of-phase) stretching vibration (mode 45). In the Raman spectrum, the band attributed to the symmetric Pt−Cl stretch has a larger intensity than that associated with the antisymmetric Pt−Cl stretching mode. In the infrared spectrum, the relative intensities of the corresponding modes 44 and 45 are reversed.

A very similar assignment of the Pt−Cl symmetric and antisymmetric stretching vibrations was reported for cisplatin, these modes were assigned at 324 and 318 cm^{-1}, respectively, in the Raman spectrum.[32]

The question arises what is the reason of the splitting of the ν(Pt−Cl) bands in the spectra of picoplatin? It seems that there are two combined reasons. First, due to strong intermolecular hydrogen bonds in the crystal, the two platinum-chloride bond lengths are different [2.299(2) and 2.322(2) Å].[12] Second, a factor group splitting (also called Davydov effect) affects the spectra. The title complex crystallizes in a monoclinic system, $P2_1/c$ (C_{2h}^5), with four molecules in the unit cell ($Z = 4$). Thus, a coupling may occur between various Pt−Cl stretching

dx.doi.org/10.1021/jp5056254 | J. Phys. Chem. A 2014, 118, 6922−6934

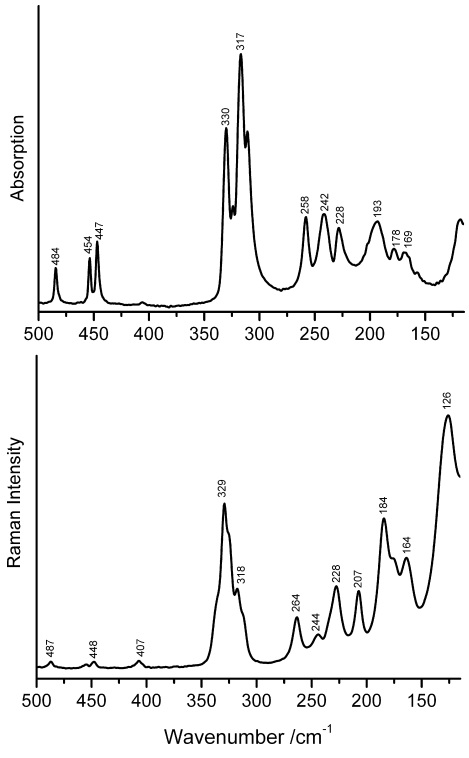

Figure 4. Comparison of the experimental FT-IR spectrum (upper part) and FT-Raman spectrum (lower part) of picoplatin (range 500–100 cm^{1}).

vibrations of four molecules within the unit cell. The other evidence of a factor group splitting is the fact that the corresponding wavenumbers of several bands do not coincide in the IR and Raman spectra of picoplatin.

In accordance with the calculations, the band at 484 cm^{-1} in the IR spectrum can be assigned to the platinum–ammonia, ν(Pt-N2) stretching vibration (mode 41). The frequency of this mode is very well-reproduced by the mPW1PW and PBE0 methods (484 and 487 cm^{-1}, respectively).

As revealed by PED, the Pt-N(ring) stretching vibration, ν(Pt–N3), is mixed with various bending deformations and generates the medium intense bands at 242 cm^{-1} (IR, mode 47) and 207 cm^{-1} (Raman, mode 49). The band at 228 cm^{-1} in the IR and Raman spectra (mode 48) involves a large contribution from the δ(Pt–N3) bending vibration. Thus, the bands at 242 (IR), 228 (IR/Raman), and 207 cm^{-1} (Raman) can be considered as the spectral markers for the Pt–N(ring) bond in picoplatin.

The δ(Cl–Pt–Cl) in-plane bending vibration (mode 53) can be attributed to the medium intensity band at 164 cm^{-1}, in the Raman spectrum of picoplatin (Figure 4). For cisplatin, this vibration was unambiguously assigned to the prominent Raman band at 163 cm^{-1}.[28,32] In the PBE0/III calculations, the theoretical frequencies of the δ(Cl–Pt–Cl) bending mode are very similar for picoplatin (141 cm^{-1}) and cisplatin (146 cm^{-1}).[32] Both calculated values refer to the compounds in the gas phase. However, in the experimental spectra of the platinum(II) complexes, the corresponding frequencies show an upward shift due to intermolecular interactions in the solid compounds.

It is expected that in the spectra of solid picoplatin, the frequency of the mode involving $\tau(NH_3)$ torsion will show a pronounced upward shift, in comparison to the corresponding theoretical value since this mode is strongly affected by the N–H···Cl intermolecular hydrogen bonds (not included in the calculations). Thus, in the spectrum of picoplatin, in the range below 200 cm^{-1}, the differences between the theoretical and experimental wanumbers of the bands are inevitable.

Performance of DFT Methods for the Calculations of the Platinum–Ligand Modes. Table 5 lists the selected unscaled frequencies of the Pt–ligand vibrations computed by the mPW1PW, PBE0, B3LYP, CAM-B3LYP, and LC-ωPBE density functional methods.

Figure 5 compares the experimental IR spectrum of picoplatin, in the 550–150 cm^{-1} region, with the corresponding theoretical IR spectra calculated by the B3LYP, CAM-B3LYP, LC-ωPBE, and PBE0 density functional methods using the III basis set. It is clear that the B3LYP method predicts too low frequency (by about 20 cm^{-1}) for the $\nu(Pt–NH_3)$ stretching vibration (mode 41), in comparison to the experiment.

As is seen in Table 5, the LC-ωPBE functional overestimates (by about 15 cm^{-1}) the $\nu(Pt-NH_3)$ stretching frequency. The remaining DFT methods give excellent results: the calculated frequencies are 484 cm^{-1} (CAM-B3LYP and mPW1PW) and 487 cm^{-1} (PBE0), which reproduce the experiment, 484 (IR) and 487 cm^{-1} (Raman).

In the reported study on cisplatin,[32] the results obtained by the B3LYP method for the $\nu(Pt–NH_3)$ stretching modes also showed significant discrepancies with experiment, the two ν(Pt–N) stretching vibrations were assigned at 524 and 509 cm^{-1}, respectively, whereas the calculations performed at the

Table 5. Comparison of the Experimental Metal-Ligand Vibrational Bands with the Theoretical Unscaled Frequencies, ν (cm^{-1}), IR Intensities[a], I_{IR} (km mol^{-1}) and Raman Scattering Activities[a], S_R ($Å^4$ amu^{-1}) of Picoplatin Calculated by the mPW1PW, PBE0, B3LYP, CAM-B3LYP, and LC-ωPBE Methods Using the III Basis Set.

no.	IR	Raman	mPW1PW	PBE0	B3LYP	CAM-B3LYP	LC-ωPBE	predominant vibration[b]
41	484 m	487 w	484 [9, 6]	487 [8, 6]	464 [10, 4]	484 [9, 5]	499 [9, –]	ν (Pt–N2)
44	330 vs	329 s	341 [25, 10]	342 [25, 10]	327 [25, 12]	342 [27, 10]	354 [29, –]	ν_s (Pt–Cl)
45	317 vs	318 m	329 [36, 9]	330 [36, 9]	316 [35, 11]	330 [38, 9]	342 [39, –]	ν_a (Pt–Cl)
47	242 m	244 w	238 [6, 1]	239 [6, 1]	230 [5, 1]	237 [6, 1]	243 [7, –]	δ(Cl5–Pt–N3), ν(Pt–N3)
48	228 m	228 m	218 [5, 1]	219 [5, 1]	213 [5, 1]	218 [5, 1]	221 [5, –]	π_s Pt, δ(Pt–N3)
49	202 sh	207 m	201 [1, 1]	202 [1, 1]	194 [1, 1]	201 [1, 1]	204 [1, –]	ν(Pt–N3)
53	164 sh	164 m	141 [1, 2]	141 [1, 2]	137 [1, 2]	141 [1, 2]	144 [2, –]	δ(Cl–Pt–Cl)

[a]The calculated IR intensities and Raman scattering activities are the first and second numbers, respectively, in square brackets. [b]Abbreviations are under Table 4.

dx.doi.org/10.1021/jp5056254 | J. Phys. Chem. A 2014, 118, 6922–6934

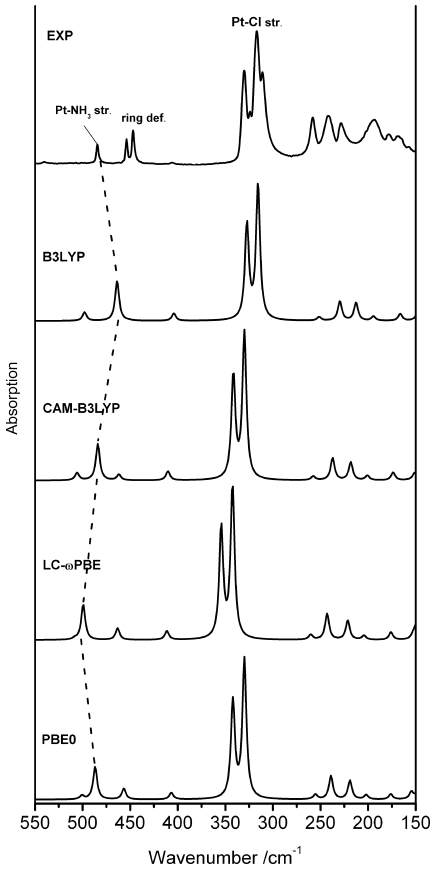

Figure 5. Comparison between the experimental IR spectrum of picoplatin (range 550−150 cm^{-1}) and the corresponding theoretical IR spectra calculated by the B3LYP, CAM-B3LYP, LC-ωPBE, and PBE0 density functional methods using the III basis set (the theoretical frequencies are unscaled).

B3LYP/SDD/D95V(d,p) level predicted these frequencies at 459 and 450 cm^{-1}, respectively.

Thus, the results obtained for picoplatin and cisplatin indicate that the B3LYP method is deficient in the prediction of the strength of the Pt←NH_3 coordination bond in platinum(II) complexes. On the other hand, the B3LYP performs very well for the ν(Pt−Cl) stretching modes in picoplatin. The B3LYP-calculated frequencies of the symmetric and antisymmetric Pt−Cl stretching vibrations are 327 and 316 cm^{-1}, respectively, while the corresponding IR bands were observed at 330 and 317 cm^{-1} (neglecting band splitting). The LC-ωPBE method overestimated these frequencies by about 25 cm^{-1}, while the remaining functionals gave slightly too high frequencies (by about 11−13 cm^{-1}).

The Raman band at 207 cm^{-1} arises mainly from the Pt−N(ring) stretching vibration (mode 49). The B3LYP method predicted too low a frequency (194 cm^{-1}) for this mode, whereas all the other DFT methods yielded very good agreement with the experiment.

As follows from Table 5, the PBE0, mPW1PW, and CAM-B3LYP methods yield very similar results and show the best overall performance in the prediction of the frequencies of the Pt−ligand vibrational modes.

CONCLUSIONS

In this work, we present for the first time the FT-Raman and FT-IR spectra of picoplatin, *cis*-[$PtCl_2(NH_3)$(2-picoline)], which is a new promising anticancer agent with high efficacy against many tumors and greatly reduced toxicity, in comparison to cisplatin. The comprehensive theoretical studies on the molecular structure, the nature of Pt−ligand bonding, vibrational frequencies, and intensities were performed. We have also investigated the performance of different DFT methods, including hybrid (PBE0, mPW1PW, and B3LYP) and long-range corrected hybrid density functionals (LC-ωPBE and CAM-B3LYP) in the prediction of the molecular structure and vibrations of picoplatin. Various effective core potentials (ECP) and basis sets have been used.

The main conclusions obtained in this study can be summarized as follows: (1) In the prediction of the molecular structure of picoplatin, the best results have been obtained by LC-ωPBE, followed by PBE0, mPW1PW, and CAM-B3LYP density functionals, while the least accurate is B3LYP. The use of the LanL2TZ(f) ECP/basis set for Pt, in conjunction with all tested DFT methods, improves the calculated geometry of the title complex. (2) The PBE0, mPW1PW, and CAM-B3LYP density functionals show the best performance in the prediction of the frequencies of the Pt−ligand vibrations. Moreover, these methods give very good overall agreement between the calculated and experimental vibrational spectra of picoplatin. (3) The B3LYP functional is deficient in the calculations of the Pt−N stretching modes (the predicted frequencies are too low); however, it yields accurate frequencies of the ν(Pt−Cl) stretching vibrations. The LC-ωPBE0 method overestimates the frequencies of the ν(Pt−Cl) and ν(Pt−NH_3) stretching vibrations. (4) In the Raman spectrum of picoplatin, the most prominent bands at 1043, 804, and 562 cm^{-1} are the "marker bands" for the picoline ligand bound to platinum. In the IR spectrum, the most intense peaks at 778 and 717 cm^{-1} arise from the picoline ring torsions coupled with the C−H out-of-plane bending vibrations, while the very strong band at 1479 cm^{-1} is due to the C−H in-plane bending mixed with the ring stretching vibrations. (5) The "spectral signature" of the ammonia ligand in picoplatin is the very strong band at 1324 cm^{-1} in the IR spectrum. This peak is associated with the $\delta_s(NH_3)$ symmetric bending vibration, also called the NH_3 umbrella mode. We suggest that this mode is probably a large-amplitude vibration (LAV), therefore, it is impossible to predict the wavenumber and IR intensity of this mode, neither in the harmonic nor in the anharmonic approximations. (6) The band at 330/329 cm^{-1} (IR/Raman) is due to the ν_s(Pt−Cl) symmetric stretching vibration, while the band at 317/318 cm^{-1} (IR/Raman) arises from the ν_a(Pt−Cl) antisymmetric stretching vibration. (7) The band at 484 cm^{-1} in the IR spectrum is assigned to the ν(Pt−NH_3) stretching vibration in picoplatin. (8) The medium intensity bands at 242 (IR), 228 (IR/Raman), and 207 cm^{-1} (Raman) can be considered as the marker bands for the Pt−N(ring) bond in picoplatin. (9) The obtained results are important for investigation on drug−target interactions using vibrational spectroscopy and for further spectroscopic and structural studies on new molecular systems containing picoplatin.

ASSOCIATED CONTENT

Supporting Information

Table S1 collects internal coordinates for picoplatin used in normal coordinate analysis. Table S2 contains natural atomic charges for picoplatin and cisplatin. Table S3 lists all theoretical frequencies and spectral intensities calculated by the tested DFT methods. Figure S1 shows the mean percent deviations

dx.doi.org/10.1021/jp5056254 | J. Phys. Chem. A 2014, 118, 6922−6934

for the calculated Pt−ligand bond lengths. This material is available free of charge via the Internet at http://pubs.acs.org.

AUTHOR INFORMATION

Corresponding Author

*E-mail: danuta.michalska@pwr.edu.pl. Tel: +48 71 3203759. Fax: +48 71 3202440.

Notes

The authors declare no competing financial interest.

ACKNOWLEDGMENTS

The work was financed by a statutory activity subsidy from the Polish Ministry of Science and Higher Education for the Faculty of Chemistry of Wrocław University of Technology. We gratefully acknowledge the instrumental grant 6221/IA/119/2012 from Polish Ministry of Science and Higher Education, which supported our Integrated Laboratory of Research and Engineering of Advanced Materials where the IR and Raman measurements were performed. The generous computer time from the Wroclaw Supercomputer and Networking Center as well as Poznan Supercomputer and Networking Center is acknowledged.

REFERENCES

(1) Rosenberg, B.; Van Camp, L.; Trosko, J. E.; Mansour, V. H. Platinum Compounds: A New Class of Potent Antitumour Agents. *Nature* **1969**, *222*, 385−386.

(2) Rabik, C. A.; Dolan, M. E. Molecular Mechanisms of Resistance and Toxicity Associated with Platinating Agents. *Cancer Treat. Rev.* **2007**, *33*, 9−23.

(3) Neidle, S.; Ismail, I. M.; Sadler, P. J. The Structure of the Antitumor Complex cis-(Diammino) (1,1-cyclobutanedicarboxylato)-Pt(II): X Ray and NMR Studies. *J. Inorg. Biochem.* **1980**, *13*, 205−212.

(4) Boulikas, T.; Vougiouka, M. Cisplatin and Platinum Drugs at the Molecular Level. *Oncol. Rep.* **2003**, *10*, 1663−1682.

(5) Wheate, N. J.; Walker, S.; Craig, G. E.; Oun, R. The Status of Platinum Anticancer Drugs in the Clinic and in Clinical Trials. *Dalton Trans.* **2010**, *39*, 8113−8127.

(6) Limited, A. I. Lobaplatin D 19466. *Drugs R&D* **2003**, *4*, 369−372.

(7) Lee, J.-W.; Park, J.-K.; Lee, S.-H.; Kim, S.-Y; Cho, Y.-B.; Kuh, H.-J. Anti-Tumor Activity of Heptaplatin in Combination with 5-Fluorouracil or Paclitaxel Against Human Head and Neck Cancer Cells In Vitro. *Anti-Cancer Drugs* **2006**, *17*, 377−384.

(8) Kelland, L. The Resurgence of Platinum-Based Cancer Chemotherapy. *Nat. Rev. Cancer* **2007**, *7*, 573−584.

(9) Rogers, P.; Boxall, F. E.; Allott, C. P.; Stephens, T. C.; Kelland, L. R. Sequence-Dependent Synergism Between the New Generation Platinum Agent ZD0473 and Paclitaxel in Cisplatin-Sensitive and -Resistant Human Ovarian Carcinoma Cell Lines. *Eur. J. Cancer* **2002**, *38*, 1653−1660.

(10) Sharp, S. Y.; O'Neill, C. F.; Rogers, P.; Boxall, F. E.; Kelland, L. R. Retention of Activity by the New Generation Platinum Agent AMD0473 in Four Human Tumour Cell Lines Possessing Acquired Resistance to Oxaliplatin. *Eur. J. Cancer* **2002**, *38*, 2309−2315.

(11) Raynaud, F. I.; Boxall, F. E.; Goddard, P. M.; Valenti, M.; Jones, M.; Murrer, B. A.; Abrams, M.; Kelland, L. R. Cis-Amminedichloro(2-methylpyridine)platinum(II) (AMD473), a Novel Sterically Hindered Platinum Complex: In Vivo Activity, Toxicology, and Pharmacokinetics in Mice. *Clin. Cancer Res.* **1997**, *3*, 2063−2074.

(12) Chen, Y.; Guo, Z.; Parsons, S.; Sadler, P. J. Stereospecific and Kinetic Control over the Hydrolysis of a Sterically Hindered Platinum Picoline Anticancer Complex. *Chem.−Eur. J.* **1998**, *4*, 672−676.

(13) Chen, Y.; Guo, Z.; Parkinson, P. J.; Sadler, P. J. Kinetic Control of Reactions of a Sterically Hindered Platinum Picoline Anticancer Complex with Guanosine 5′-Monophosphate and Glutathione. *J. Chem. Soc., Dalton Trans.* **1998**, 3577−3585.

(14) Sarmah, P.; Deka, R. C. Hydrolysis and Binding Mechanism of AMD473 (cis-[$PtCl_2(NH_3)$(2-picoline)]) with Guanine: a Quantum Mechanical Study. *J. Mol. Struct.: THEOCHEM* **2010**, *955*, 53−60.

(15) Banerjee, S.; Sengupta, P. S.; Mukherjee, A. K. A Detailed Theoretical DFT Study of the Hydrolysis Mechanism of Orally Active Anticancer Drug ZD0473. *Chem. Phys. Lett.* **2010**, *487*, 108−115.

(16) Melchior, A.; Marcos, E. S.; Pappalardo, R. R.; Martinez, J. M. Comparative Study of the Hydrolysis of a Third- and a First-Generation Platinum Anticancer Complexes. *Theor. Chem. Acc.* **2011**, *128*, 627−638.

(17) Sarmah, P.; Deka, R. C. Stability and Proton Transfer in DNA Base Pairs of AMD473-DNA Adduct. *Chem. Phys. Lett.* **2011**, *508*, 295−299.

(18) Chen, Y.; Parkinson, J. A.; Guo, Z.; Brown, T.; Sadler, P. J. A New Platinum Anticancer Drug Forms a Highly Stereoselective Adduct with Duplex DNA. *Angew. Chem., Int. Ed.* **1999**, *38*, 2060−2063.

(19) Ravera, M.; Gabano, E.; Zanellato, I.; Bonarrigo, I.; Escribano, E.; Moreno, V.; Font-Bardia, M.; Calvet, T.; Osella, D. Synthesis, Characterization and Antiproliferative Activity on Mesothelioma Cell Lines of bis(Carboxylato)platinum(IV) Complexes Based on Picoplatin. *Dalton Trans.* **2012**, *41*, 3313−3320.

(20) Pažout, R.; Maixner, J.; Hrda, M.; Loužilova, T.; Kačer, P. A Bromine Analog of Picoplatin: A New Substance from the Group of Platinum-Based Chemotherapeutics. *Acta Crystallogr., Sect. C: Cryst. Struct. Commun.* **2013**, *69*, 337−339.

(21) Zvereva, E.; Shagidullin, A. R.; Katsyuba, S. A. Ab Initio and DFT Predictions of Infrared Intensities and Raman Activities. *J. Phys. Chem. A* **2011**, *115*, 63−39.

(22) Barone, V.; Biczysko, M.; Bloino, J. Fully Anharmonic IR and Raman Spectra of Medium-Size Molecular Systems: Accuracy and Interpretation. *Phys. Chem. Chem. Phys.* **2014**, *16*, 1759−1787.

(23) Wysokiński, R.; Michalska, D. The Performance of Different Density Functional Methods in the Calculation of Molecular Structures and Vibrational Spectra of Platinum(II) Antitumour Drugs: Cisplatin and Carboplatin. *J. Comput. Chem.* **2001**, *22*, 901−912.

(24) Adamo, C.; Barone, V. Exchange Functionals with Improved Long Range Behaviour and Adiabatic Connection Methods without Adjustable Parameters. The mPW and mPW1PW Models. *J. Chem. Phys.* **1998**, *108*, 664−675.

(25) Michalska, D.; Wysokiński, R. The Prediction of Raman Spectra of Platinum(II) Anticancer Drugs by Density Functional Theory. *Chem. Phys. Lett.* **2005**, *403*, 211−217.

(26) Wysokiński, R.; Kuduk-Jaworska, J.; Michalska, D. Electronic Structure, Raman and Infrared Spectra, and Vibrational Assignment of Carboplatin. *J. Mol. Struct. (Theochem)* **2006**, *758*, 169−179.

(27) Wysokiński, R.; Hernik, K.; Szostak, R.; Michalska, D. Electronic Structure and Vibrational Spectra of cis-Diammine(orotato)platinum-(II), a Potential Cisplatin Analogue; DFT and Experimental Study. *Chem. Phys.* **2007**, *333*, 37−48.

(28) Amado, A. M.; Fiuza, S. M.; Marques, M. P. M.; Batista de Carvalho, L. A. E. Conformational and Vibrational Study of Platinum(II) Anticancer Drugs: Cis-Diamminedichloroplatinum(II) as a Case Study. *J. Chem. Phys.* **2007**, *127*, 185104−185113.

(29) Fiuza, S. M.; Amado, A. M.; Marques, M. P. M.; Batista de Carvalho, L. A. E. Use of Effective Core Potential Calculations for the Conformational and Vibrational Study of Platinum(II) Anticancer Drugs. Cis-Diamminedichloroplatinum(II) as a Case Study. *J. Phys Chem. A* **2008**, *112*, 3253−3259.

(30) De Berrêdo, R. C.; Jorge, F. E.; Jorge, S. S.; Centoducatte, R. An Augmented Gaussian Basis Set for Calculations of Molecular Polarizabilities on Platinum Compounds. *Comput. Theor. Chem.* **2011**, *965*, 236−239.

(31) Paschoal, D.; Marcial, B. L.; Lopes, J. F.; De Almeida, W. B.; Dos Santos, H. F. The Role of the Basis Set and the Level of Quantum

Mechanical Theory in the Prediction of the Structure and Reactivity of Cisplatin. *J. Comput. Chem.* **2012**, *33*, 2292−2302.
(32) Malik, M.; Michalska, D. Assessment of New DFT Methods for Predicting Vibrational Spectra and Structure of Cisplatin: Which Density Functional Should We Choose for Studying Platinum(II) Complexes? *Spectrochim. Acta, Part A* **2014**, *125*, 431−439.
(33) Battle, A. R.; Choi, R.; Hibbs, D. E.; Hambley, T. W. Platinum(IV) Analogues of AMD473 (cis-[PtCl2(NH3)(2-picoline)]): Preparative, Structural, and Electrochemical Studies. *Inorg. Chem.* **2006**, *45*, 6317−6322.
(34) Murrer, B. A. Platinum Complexes. U.S. Patent 5665771, September 9, 1997.
(35) Yanai, T.; Tew, D. P.; Handy, N. C. A New Hybrid Exchange-Correlation Functional Using the Coulomb-Attenuating Method (CAM-B3LYP). *Chem. Phys. Lett.* **2004**, *393*, 51−57.
(36) Vydrov, O. A.; Scuseria, G. E. Assessment of a Long-Range Corrected Hybrid Functional. *J. Chem. Phys.* **2006**, *125*, 234109−234109−9.
(37) Perdew, J. P.; Wang, Y. Accurate and Simple Analytic Representation of the Electron-Gas Correlation Energy. *Phys. Rev. B* **1992**, *45*, 13244−13249.
(38) Perdew, J. P.; Burke, K.; Ernzerhof, M. Generalized Gradient Approximation Made Simple. *Phys. Rev. Lett.* **1996**, *77*, 3865−3868.
(39) Ernzerhof, M.; Scuseria, G. E. Assessment of the Perdew-Burke-Ernzerhof Exchange-Correlation Functional. *J. Chem. Phys.* **1999**, *110*, 5029−5036.
(40) Adamo, C.; Barone, V. Toward Reliable Density Functional Methods without Adjustable Parameters: The PBE0 Model. *J. Chem. Phys.* **1999**, *110*, 6158−6170.
(41) Becke, A. D. Density-Functional Thermochemistry. III. The Role of Exact Exchange. *J. Chem. Phys.* **1993**, *98*, 5648−5652.
(42) Lee, C.; Yang, W.; Parr, R. G. Development of the Colle-Salvetti Correlation-Energy Formula into a Functional of the Electron Density. *Phys. Rev. B* **1988**, *37*, 785−789.
(43) Hay, P. J.; Wadt, W. R. Ab Initio Effective Core Potentials for Molecular Calculations. Potentials for the Transition Metal Atoms Sc to Hg. *J. Chem. Phys.* **1985**, *82*, 270−283.
(44) Andrae, D.; Haussermann, U.; Dolg, M.; Stoll, H.; Preuss, H. Energy-Adjusted Ab Initio Pseudopotentials for the Second and Third Row Transition Elements. *Theor. Chim. Acta* **1990**, *77*, 123−141.
(45) Bergner, A.; Dolg, M.; Kuechle, W.; Stoll, H.; Preuss, H. Ab Initio Energy-Adjusted Pseudopotentials for Elements of Groups 13−17. *Mol. Phys.* **1993**, *80*, 1431−1441.
(46) Roy, L. E.; Hay, P. J.; Martin, R. L. Revised Basis Sets for the LANL Effective Core Potentials. *J. Chem. Theory Comput.* **2008**, *4*, 1029−1031.
(47) Dunning, T. H. Jr.; Hay, P. J. In *Modern Theoretical Chemistry*; Schaefer H. F. III, Ed.; Plenum Press: New York, Volume *4*, 1976.
(48) Helios, K.; Wysokiński, R.; Zierkiewicz, W.; Proniewicz, L. M.; Michalska, D. Unusual Noncovalent Interaction Between the Chelated Cu(II) Ion and the π Bond in the Vitamin B_{13} Complex, *cis*-Diammine(orotato)copper(II): Theoretical and Vibrational Spectroscopy Studies. *J. Phys. Chem. B* **2009**, *113*, 8158−8169.
(49) Helios, K.; Pietraszko, A.; Wysokiński, R.; Strommen, D. P.; Michalska, D. A Novel Complex of Orotic Acid (Vitamin B_{13}) with Nickel, $[Ni(HOr)(NH_3)_2(H_2O)_2]$: Crystal Structure, Vibrational Spectra and Density Functional Study. *Vib. Spectrosc.* **2010**, *52*, 1−9.
(50) Helios, K.; Wysokiński, R; Pietraszko, A.; Michalska, D. Vibrational Spectra and Reinvestigation of the Crystal Structure of a Polymeric Copper(II)−Orotate Complex, $[Cu(\mu\text{-}HOr)(H_2O)_2]_n$: The Performance of New DFT Methods, M06 and M05−2X, in Theoretical Studies. *Vib. Spectrosc.* **2011**, *55*, 207−215.
(51) Frisch, M. J.; Trucks, G. W.; Schlegel, H. B.; Scuseria, G. E.; Robb, M. A.; Cheeseman, J. R.; Scalmani, G.; Barone, V.; Mennucci, B.; Petersson, et al. *Gaussian 09*, Gaussian, Inc.: Wallingford, CT, 2009.
(52) Reed, A. E.; Curtiss, L. A.; Reinhold, F. Intermolecular Interactions from a Natural Bond Orbital, Donor-Acceptor Viewpoint. *Chem. Rev.* **1988**, *88*, 899−926.
(53) Glendening, E. D.; Badenhoop, J. K.; Reed, A. E.; Carpenter, J. E.; Bohmann, J. A.; Morales, C. M.; Weinhold, F. *NBO 5.0 Software*; Theoretical Chemistry Institute, University of Wisconsin: Madison, WI, 2001.
(54) Halls, M. D.; Velkovski, J.; Schlegel, H. B. Harmonic Frequency Scaling Factors for Hartree-Fock, S-VWN, B-LYP, B3-LYP, B3-PW91 and MP2 with the Sadlej pVTZ Electric Property Basis Set. *Theor. Chem. Acc.* **2001**, *105*, 413−421.
(55) Balci, K.; Akkaya, Y.; Akyuz, S.; Palavan-Unsal, N. DFT and MP2 Based Quantum Mechanical Calculations and a Theoretical Vibrational Spectroscopic Investigation on Roscovitine, a Potential Drug to Treat Cancers. *J. Raman Spectrosc.* **2011**, *42*, 719−732.
(56) Merrick, J. P.; Moran, D.; Radom, L. An Evaluation of Harmonic Vibrational Frequency Scale Factors. *J. Phys. Chem. A* **2007**, *111*, 11683−11700.
(57) Nowak, M. J.; Lapinski, L.; Bieńko, D. C.; Michalska, D. Infrared Matrix Isolation Spectra of 1-Methyluracil. Revised Assignment Based on the Hartree-Fock and post-Hartree-Fock Studies. *Spectrochim. Acta, Part A* **1997**, *53*, 855−865.
(58) Rostkowska, H.; Lapinski, L.; Nowak, M. J. Analysis of the Normal Modes of Molecules with D_{3h} Symmetry. Infrared Spectra of Monomeric s-Triazine and Cyanuric Acid. *Vib. Spectrosc.* **2009**, *49*, 43−51.
(59) Fogarasi, G.; Zhou, X.; Taylor, P. W.; Pulay, P. The Calculation of Ab Initio Molecular Geometries: Efficient Optimization by Natural Internal Coordinates and Empirical Correction by Offset Forces. *J. Am. Chem. Soc.* **1992**, *114*, 8191−8201.
(60) Long, D. A. *Raman Spectroscopy*; McGraw-Hill: New York, 1977.
(61) Morzyk-Ociepa, B.; Nowak, M. J.; Michalska, D. Vibrational Spectra of 1-Methylthymine: Matrix Isolation, Solid State and Theoretical Studies. *Spectrochim. Acta, Part A* **2004**, *60*, 2113−2123.